Neuropsychiatric Disease and Treatment

Dovepress

open access to scientific and medical research

Open Access Full Text Article

ORIGINAL RESEARCH

RETRACTED ARTICLE: Protective Role of Astrocyte-Derived Exosomal *microRNA-361* in Cerebral Ischemic-Reperfusion Injury by Regulating the *AMPK/mTOR* Signaling Pathway and Targeting *CTSB*

This article was published in the following Dove Press journal:
Neuropsychiatric Disease and Treatment

Xiancong Bu[1]
Dong Li[2]
Feng Wang[1]
Qimeng Sun[1]
Zixian Zhang[1]

[1]Department of Neurology, Zaozhuang Municipal Hospital, Zaozhuang, Shandong 277100, People's Republic of China; [2]Department of Neurology, Zaozhuang Hospital of Zaozhuang Mining Group, Zaozhuang, Shandong 277100, People's Republic of China

Background: Evidence has shown that microRNAs (miRNAs) are implicated in ischemic diseases. Therefore, the aim of the present study was to identify the functions of astrocyte (ATC)-derived exosomal *miR-361* on cerebral ischemic-reperfusion (I/R) injury.

Methods: A rat model of cerebral I/R injury was initially established, followed by injection of ATC-derived exosomes. Next, the protective function of ATC-derived exosomes in rats with cerebral I/R injury was evaluated, and then the effect of *miR-361* on rats with cerebral I/R injury was evaluated by changing *miR-361* expression in exosomes. PC12 cells that underwent oxygen-glucose deprivation/reoxygenation were used to simulate I/R in vitro. The effect of ATC-derived exosomal *miR-361* on the viability and apoptosis of OGD/R-treated PC12 cells was also assessed. The bioinformatics analysis predicted the targeted gene of *miR-361*.

Results: It was found that I/R was damaging to the brain nerves of rats, while ATC-derived exosomal *miR-361* relieved nerve damage caused by I/R. Furthermore, the in vitro experiments demonstrated that ATC-derived exosomal *miR-361* increased OGD/R-inhibited PC12 cell viability and suppressed cell apoptosis. Bioinformatics predicted that *miR-361* targeted cathepsin B (*CTSB*). *CTSB* upregulation blocked the protective roles of *miR-361*. In addition, *miR-361* was found to downregulate the *AMPK/mTOR* signaling pathway by targeting *CTSB*.

Conclusion: The present study demonstrated that ATC-derived exosomal *miR-361* alleviates nerve damage in rats with cerebral I/R injury by targeting *CTSB* and downregulating the *AMPK/mTOR* pathway. This may offer novel insights into treatment for I/R injury.

Keywords: cerebral ischemic-reperfusion injury, astrocyte, exosome, *microRNA-361*, *AMPK/mTOR* signaling pathway, cathepsin B

Introduction

Ischemic stroke is regarded as a complicated disease comprising of a group of heterogeneous disorders that result from various genetic and environmental risk factors.[1] Ischemic stroke often involves blood-brain barrier disruption in the infarct region, or a decline in local blood flow or metabolism.[2] Currently, the main clinical regimen for ischemic stroke depends on re-perfusing the ischemic area via drugs or early thrombolysis, thereby restoring oxygen and glucose supply,[3] which therefore gives rise to ischemic-reperfusion (I/R) injury.[4] Cerebral I/R injury is known as brain tissue deterioration as a result of ischemia, which simultaneously reverses the cerebral blood flow in patients with acute ischemic stroke following mechanical or

Correspondence: Zixian Zhang
Email zixianzhang1344@163.com

http://doi.org/10.2147/NDT.S260748

chemical therapies.[5] Natural compounds with the functions of anti-inflammation, anti-oxidation, anti-apoptosis and calcium antagonization, as well as neurofunctional modulation, present either preventive or therapeutic roles on cerebral I/R injury.[6] However, it remains a tough issue to treat cerebral I/R injury.[7] Therefore, it is imperative to seek eligible therapy for cerebral I/R injury treatment.

Exosomes are small membrane vesicles with a diameter of 30–100 nm, which are released into the extracellular fluids via the cells in all the living systems.[8,9] Exosomes have been revealed to alleviate oxygen-glucose deprivation (OGD)-stimulated inflammatory responses, neuronal death and the apoptotic signaling pathway changes.[10] Astrocytes (ATCs) are specific star-shaped glial cells that are responsible for extracellular ion balance, nutritional support, synaptic remodeling and blood-brain barrier formation.[11] ATC-secreted exosomes carry neuroprotective loads to execute neuroprotective function.[12,13] Evidence has shown that microRNAs (miRNAs) are implicated in the etiology and progression of ischemic diseases, such as cerebral ischemia.[14] In the present study, the microarray analysis identified an enrichment of *miR-361* in ATC-derived exosomes. A previous study revealed that *miR-361*-modulated prohibitin suppress mitochondrial fission and apoptosis, which protected th heart from ischemic injury.[15] *miR-361-5p* has been identified as one of the top five cerebral cavernous m formations-relevant miRNAs.[16] miRNAs are well known to induce translational repression by binding to their c mentary target mRNAs.[17] The present stu identified athepsin B (*CTSB*) as a target of *miR-361*. *CTSB* is a lysosomal cysteine protease and leads the neurona ell death after focal and global cerebr ischemia in animal settings.[18] *CTSB* activation, under athological conditions, can result in cellular apopto autoly excess e autophagy, as well as damage t neighb ring ce [19] Therefore, the present study hypo esized ATC-derived exosomal *miR-361* exerts protecti roles in cerebral I/R injury, with both in vivo and in vit experiments performed to validate the hypothesis and to identify the potential molecules.

Materials and Methods

Ethics Statement

Animals were treated humanely with the approved procedures based on the recommendations in the Guide for the Care and Use of Laboratory Animals of the National Institutes of Health. The protocol was issued by the Institutional Animal Care and Use Committee of Zaozhuang Municipal Hospital (#201803017).

ATC Culture and Treatment

Rat ATCs (RRID: CVCL_E150) were purchased from the Cell Biology Institute of Chinese Academy of Sciences (Shanghai, China). The medium was high-glucose DMEM containing 10% fetal bovine serum (FBS) (Gibco Company, Grand Island, NY, USA). *miR-361* inhibitor and miR-negative control (NC) were purchased from Shanghai GenePharma Co., Ltd. The inhibitor or NC vector was transfected into ATCs at dose of 0 ng using a Lipofectamine® 2000 trans tion kit (vitrogen; Thermo Fisher Scientific, In). The ells were correspondingly named the ATC inhibitor grou ATC-Mock group. An equal volum of ph iological saline was administered to ATCs a bla group, ich was named the ATC-Saline g After 48 transfection, the cells were collected for s sequent experiments. The exosomes extract m the ATC inhibitor group were termed Exo-Inhi tor, while those extracted from the ATC-Empty gro were term Exo-Mock.

Exoso eparation

A t passage 2 to 3 in each group were washed twice ith phosphate-buffered saline (PBS), and cultured for 48–72 h in serum-free medium instead of 10% FBS-supplemented one. Then, the cell supernatant was collected, and the exosomes were extracted by differential centrifugation.[20] All centrifugal steps were operated at 4°C and the other procedures were operated on ice. The precipitate was resuspended in PBS, followed by centrifugation another two times, and the precipitate, again, was resuspended in 50–100 μL PBS and stored at −80°C for use. The size and shape of the extracted exosomes were identified by Nanosight and transmission electron microscopy observation. Western blot analysis was used to identify exosomal marker proteins. Protein concentration of the extracted exosomes was determined by a bicinchoninic acid kit, and then the exosomes were diluted to 30 μg/mL in PBS for further use.

Western Blot Analysis

The extraction of the total protein was performed via radioimmunoprecipitation assay lysis buffer embodying phenylmethylsulfonyl fluoride (Beyotime Institute of Biotechnology, Shanghai, China). The protein level in the supernatant was detected via the BCA method. Equal

volumes of protein (50 mg) were separated via SDS-PAGE (10% gel) and then transferred onto the polyvinylidene fluoride (PVDF) membrane (EMD Millipore). The PVDF membranes were incubated with tris-buffered saline tween (TBST; Boster Biological Technology Co., Ltd.) supplemented with 5% skimmed milk to block the non-specific binding. Next, the membranes were cultured with the primary antibodies (Table 1) at 4°C overnight, together with rabbit anti-rat secondary antibody for 1 h at room temperature. The proteins were developed in enhanced chemiluminescence reagent, and analyzed by BioSpectrum gel imaging system (Bio-Rad Laboratories, Inc.).

Experimental Animals and Modeling

A total of 45 male Wister rats aged 6 weeks (weight, 150 ±20 g) were purchased from Experimental Animal Center of Chinese Academy of Sciences (Shanghai, China). The rats were placed in the second-class clean animal house, raised in separate cages with standard feed and free access to water. All the rats were randomly numbered and assigned into sham group, I/R group and exosome intervention group (Exo group), Exo-Mock group and Exo-Inhibitor group, with nine rats in each group. A rat model of cerebral I/R was constructed using a silicone gel-coated nylon line (φ=0.028) as previously described.[21] The rats were fasted for 12 h before surgery with only access to water. The rats were anesthetized with pentobarbital sodium (30 mg/kg) and maintained with spontaneous respiration during the operation and the rectal temperature was maintained at 36–37.5°C. The room temperature was maintained at 25°C during and after surgery.

The rats in the Exo group were injected with the corresponding exosomes. Each rat was given 2 mL exosomes (30 μg/mL) through the caudal vein twice a week for a total of 2 weeks. Rats in the sham group were injected into an equal volume of normal saline. Following evaluation of the neurological deficit score, rats were euthanized by the administration of pentobarbital sodium (120 mg/kg)[22] (https://www.avma.org/KB/Policies/Documents/euthanasia.pdf). The animal death was confirmed by the cardiac arrest, the appearance of dilated pupils, and the loss of nerve reflexes. In each group, three rats were used for 2,3,5-triphenyltetrazole chloride (TTC) staining, three for edema in brain detection, and the left hemisphere of the remaining three rats were collected. Each left hemisphere was divided into two equal parts, one of each was used for RNA and protein extraction for reverse transcription quantitative PCR (RT-qPCR) and Western blot analysis, while the other part was used for brain section preparation for Nissl staining, C-fos immunohistochemical staining and Terminal deoxynucleotidyl transferase (TdT)-mediated dUTP nick end labeling (TUNEL) assays.

Table 1 Antibodies for Western Blot Analysis

Antibody	No., Company	Dilution Ratio
Alix	ab117600, Abcam	1: 100
CD63	ab217345, Abcam	1: 100
CD9	ab92726, Abcam	1: 100
CD81	ab79559, Abcam	1: 5000
GAPDH	ab181602, Abcam	1: 50
β-actin	ab179467, Abcam	1: 5000
Cleaved caspase-3	ab2302, Abcam	1:50
Cleaved PARP	ab32064, Abcam	1: 5000
Secondary antibody	ab150117, Abcam	1: 5000

Abbreviations: GAPDH, glyceraldehyde-3-phosphate dehydrogenase; PARP, poly (ADP-ribose) polymerase; Abcam, Abcam Inc., Cambridge, MA, USA.

Evaluation of Neurological Damage in Rats

The degree of neurological damage in rats was determined by neurological deficit score, TTC staining, degree of brain edema, and C-fos immunohistochemical staining. Neurological deficit score in rats: 24 h after blood reperfusion, neurological deficit in rats was determined by Longa scoring criteria.[21] The degree of edema in the brain was determined by the standard brain wet weight-brain dry weight.[23] The brain was weighed immediately following the extraction and then dried at 100°C for 24 h and weighed. The degree of edema in the brain was expressed by the formula: (Wet weight - dry weight)/wet weight x 100%. The area of cerebral infarction in rats was determined by TTC staining: Rat brain tissues were extracted, washed with normal saline, and cut into slices (3-mm). Then, the slices were exposed to 1% TTC solution (Oxoid) in the dark at 37°C, fixed in 10% formaldehyde and photographed, with the non-stained area regarded as the infarct area. The experimental procedure for C-fos immunohistochemical staining was performed as reported in the literature.[24]

Nissl Staining

A total of five slices were randomly selected for Nissl staining. The sections were rinsed three times with distilled water for 5 min each time, and then stained with 1% toluidine blue for 40 min (or stained with crystal violet for

30 sec) in a 60°C incubator for further use. After washing the dye with distilled water, the sections were dehydrated in 70%, 80%, 95% and 100% ethanol, and then cleared with xylene, and finally sealed with neutral gum. The sections were observed under a light microscope (Olympus Corporation).

In vitro Model of OGD/Reoxygenation (OGD/R) Mimicking I/R Injury in Mouse Neuroblastoma Cells

Mouse neuroblastoma cell line PC12 was purchased from the Cell Biology Institute of Chinese Academy of Sciences (Shanghai, China). PC12 cells with good growth were divided into control group, OGD/R group, OGD/R-exosomes group (OGD/R-Exo group), OGD/R-Mock group (treated with exosomes that were transfected with Mock vector) and OGD/R-Inhibitor group (treated with exosomes that were transfected with *miR-361* inhibitor). After cell grouping, the culture medium of each OGD/R group was discarded, and the cells were washed once with sterile PBS, loaded into the prepared glucose-free DMEM, and cultured in a three-gas incubator for 2 h. Subsequently, the cells of each OGD/R group were removed and cultured in common medium (10% FBS + DMEM) in a common incubator (37°C; 5% CO_2; saturated humidity). Cells were harvested 48 h later for subsequent experiments.

Microarray-Based Analysis

Differential expression of miRNA in rat hippocampus was analyzed using the GeneChip™ miRNA 4.0 Array Strip (Thermo Fisher Scientific, Inc.) and all procedures were performed strictly according to the manufacturer's protocols.

RT-qPCR

Total RNA from tissues and cells were acquired with the RNAiso Plus (Takara Bio, Inc. Kyoto, Japan) and TRIzol® LS Reagent (Takara Bio, Inc.), respectively. Next, formaldehyde denaturation electrophoresis was adopted to confirm the reliability of the obtained RNA. RT-qPCR was implemented as per the manufacturer's protocol, using the PrimeScript™ RT reagent kit (Takara Bio, Inc.). The mRNA expression was determined by the protocol of the standard real-time qPCR with SYBR Premix Ex Taq (Takara Bio, Inc.) with glyceraldehyde-3-phosphate dehydrogenase (GAPDH) as a loading control. The primers are presented in Table 2.

MTT Assay

The cells with good growth in each group were assayed for cell proliferation using an MTT cell proliferation and cytotoxicity assay kit (C0009; Beyotime Institute of Biotechnology). All experiments were performed in strict accordance with the manufacturer's protocol. In brief, cells in each group were treated with 20 μL MTT (5 mg/mL; m6494; Invitrogen; Thermo Fisher Scientific, Inc.). Subsequently, the supernatant was discarded, cells were treated with DMSO, and the optical density at 490 nm was detected using an Infinite M200 microplate reader (Tecan Group Ltd.).

EdU Labeling Assay

The cells of each group at passage 3 with good growth conditions were used, and the DNA replication ability of the cells was measured using a Cell-light EdU luminescence detection kit (Guangzhou RiboBio Co., Ltd.) as per the kit instructions. In brief, cells were seeded into well plates and incubated with EdU for 60 min. Next, the cells were fixed in 4% paraformaldehyde for 20 min, treated with 3% Triton X-100, and analyzed using the Click-IT EdU software. Then, the cells were observed and photographed under a fluorescence microscope (Olympus 600), and the image was analyzed using an Image-Pro Plus software. The DAPI-positive cells (total cells) and the EdU-positive (DNA replicating) cells were calculated.

Table 2 Primer Sequences of RT-qPCR

Primers	Sequences
miR-361	F: TCACACTATATCACATTGCCAGG
	R: TATGGTTGTTCTGCTCTCTGTCTC
U6	F: GACGAATGGAAGAGCCTGAC
	R: ACGCTTCACGAATTTGCGTGTC
CTSB	F: AGATCCTGGGTGCAGACTTC
	R: GTAGAAAGGGCTGGGGAAG
GAPDH	F: ACAGTCAGCCGCATCTTCTT
	R: GACAAGCTTCCCGTTCTCAG

Abbreviations: RT-qPCR, reverse transcription-quantitative polymerase chain reaction; miR, microRNA; CTSB, cathepsin B; GAPDH, glyceraldehyde-3-phosphate dehydrogenase; F, forward; R, reverse.

Flow Cytometry

A total of $1x10^4$ PC12 cells/well were made into a suspension and stained with 50 μg/mL Annexin V-fluorescein isothiocyanate (FITC)/propidium iodide (PI) in the dark for 15 min. Then, the cell apoptosis was determined using an Annexin V apoptosis kit I (BD Biosciences) and a flow cytometer (Becton Dickinson).

TUNELWell-growing PC12 cells or the rat brain tissue sections were washed with D-Hank three times, and then the apoptosis of cells was further washed using a TUNEL apoptosis detection kit (Guangzhou RiboBio Co., Ltd.) as per the manufacturer's protocol. A total of five randomly selected areas were observed under the microscope, under which the TUNEL-positive cells present greenery nuclei. All procedures were performed in triplicate.

Dual-Luciferase Report Gene Assay

The 3′untranslated region (UTR) binding sequence of *miR-361* and *CTSB* was predicted by the online prediction software TargetScan (http://www.targetscan.org/vert_72/). *CTSB* wild type (WT) and mutant type (MT) of 3′UTR binding sequence were synthesized by Shanghai Sangon Bioengineering Co., Ltd. and inserted into pMIR-REPORT™ (Thermo Fisher Scientific, Inc.) luciferase reporter vector. WT and MT plasmids were co-transfected with *miR-361* mimic or mimic NC into H293T cells using Lipofectamine 2000 transfection kit (Invitrogen; Thermo Fisher Scientific, Inc.). After 24 h, the cells were lysed and the intensity of luciferase activity was measured using the Dual-Luciferase Reporter assay system (Promega Corp.).

Statistical Analysis

The data were analyzed using SPSS 21.0 (IBM Corp.) statistical software. Whether the data were normally distributed was established using a Kolmogorov–Smirnov test. Measurement data were expressed as mean ± standard deviation and the data between the two groups was compared using a *t*-test. Comparison among multiple groups was analyzed with one-way or two-way analysis of variance (ANOVA), and Tukey's multiple comparisons test was utilized for the pairwise comparison after ANOVA. A P-value was obtained from a two-sided test, and $P<0.05$ was considered to indicate a statistically significant difference.

Results

Identification of ATCs and Exosomes

Following observation under light microscopy and glial fibrillary acidic protein (GFAP) immunofluorescence assay, the cells used in the present study met the definition of ATCs (Figure 1A). Subsequently, exosomes were extracted and the transmission electron microscopy observation (x40000) results revealed that the extracted exosomes exhibited a cup-shaped morphology (Figure 1B). The Nanosight nanoparticle tracking analysis results demonstrated that the exosome size was ~97.6 nm (Figure 1C). The Western blot analysis results suggested that exosomes were shown carrying CD9, CD63 and Alix (Figure 1D). The BCA detection suggested that the protein concentration of the extracted exosomes was 317.63 μg/mL. According to this, the exosomes were diluted to 30 μg/mL for subsequent use.

ATC-Derived Exosomes Reduce I/R-Induced Neurological Damage in Rats

Through the neurological deficit assessment, it was revealed that exosome treatment reduced I/R-induced neurological damage in rats, presenting as decreased neurological deficit scores (Figure 2A). TTC staining showed significant decline in cerebral infarct size after exosome treatment (Figure 2B). The determination of water content in the brain of rats revealed that exosome treatment decreased the degree of cerebral edema caused by I/R (Figure 2C). Subsequently, the present study used Nissl staining to assess neuronal damage in rat brain tissue;[25] where a larger number of Nissl bodies reflect a higher neuronal activity. It was revealed that the number of Nissl bodies in the injured neurons was significantly decreased. Nissl staining showed that I/R treatment aggravated brain damage, while exosome treatment could alleviate the damage caused by I/R (Figure 2D). In addition, C-fos[26] represents a neuroactive protein. C-fos is a member of the AP-1 family that is known to be involved in the regulation of neuronal viability and necessary for neuron survival.[27] Therefore, the present study further investigated C-fos expression by immunohistochemistry staining, and the results showed that exosome treatment re-increased the C-fos level, which increased neuronal viability in rat brain (Figure 2E). Furthermore, TUNEL assay was used to detect the apoptosis level in hippocampus after I/R in rats. The results revealed that exosome treatment partially reversed the apoptosis of hippocampal neurons induced by I/R (Figure 2F).

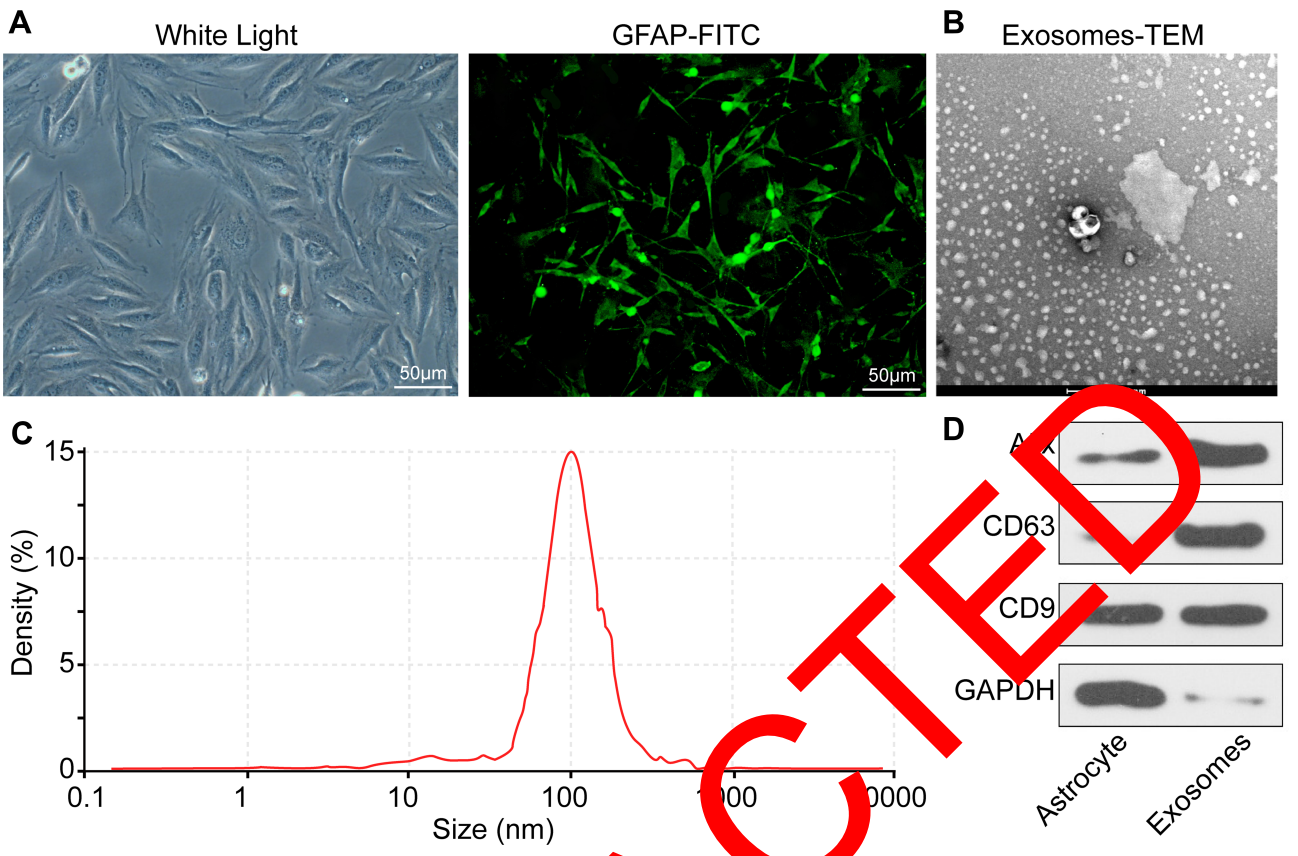

Figure 1 Identification of ATCs and exosomes. (**A**) Morphological analysis and immunofluorescence staining of ATC-specific marker GFAP showed that the cells we used were ATCs. (**B**) ATCs-derived exosomes were elliptical- or cup-shaped with a size of about 100 nm observed under a Transmission electron microscopy. (**C**) Nanosight nanoparticle tracking analysis indicated that the particle size was about 100 nm. (**D**) Exosome marker proteins CD9, CD63 and Alix determined by RT-qPCR. All experiments were performed three individual times.

Abbreviations: ATC, astrocyte; GAPDH, glyceraldehyde-3-phosphate dehydrogenase; GFAP-FITC, glial fibrillary acidic protein-fluorescein isothiocyanate.

ATC-Derived Exosomal *miR-361* Protects I/R Injury

With the aim of clarifying the mechanism of specific exosome protection, the present study used microarray to analyze the differential expression of miRNAs after exosome treatment. Based on $|\log FC| > 2$, $P < 0.05$, the present study obtained a total of 42 differentially expressed miRNAs, of which 18 were upregulated and 24 were downregulated. The heatmap revealed the top 30 differentially expressed miRNAs (Figure 3A). *miR-361*, which had the most differential expression, was selected to detect its expression level in hippocampus of each group by RT-qPCR. The results showed that the expression level of *miR-361* was significantly increased following exosome treatment (Figure 3B). To further determine the role of *miR-361*, the present study transfected *miR-361* inhibitor (miR-Inhibitor) into ATCs. The results of RT-qPCR confirmed that the transfection was successful since the *miR-361* expression in ATC was decreased after miR-inhibitor treatment (Figure 3C). Subsequently, exosomes were extracted, and the expression of *miR-361* in ATCs and exosomes was detected by RT-qPCR. The expression of *miR-361* in the exosome of the miR-Inhibitor group was significantly decreased (Figure 3D). Furthermore, I/R rats were treated with *miR-361* Inhibitor-transfected exosomes (ATC-inhibitor-exo). The results showed that decreasing exosome-loaded *miR-361* partially reversed the neuroprotective effect of ATC-derived exosomes on I/R rats. Inhibition of *miR-361* led to an increase in neurological deficit in rat brains (Figure 3E), and an aggravation in edema in rat brains (Figure 3F). The TTC staining results showed that the infarct size in rat brain tissues was increased (Figure 3G). Again, the number of Nissl bodies in brain hippocampal tissues was declined (Figure 3H), and the expression of c-fox protein was decreased (Figure 3I), but the number of TUNEL-positive cells was increased after *miR-361* inhibition (Figure 3J).

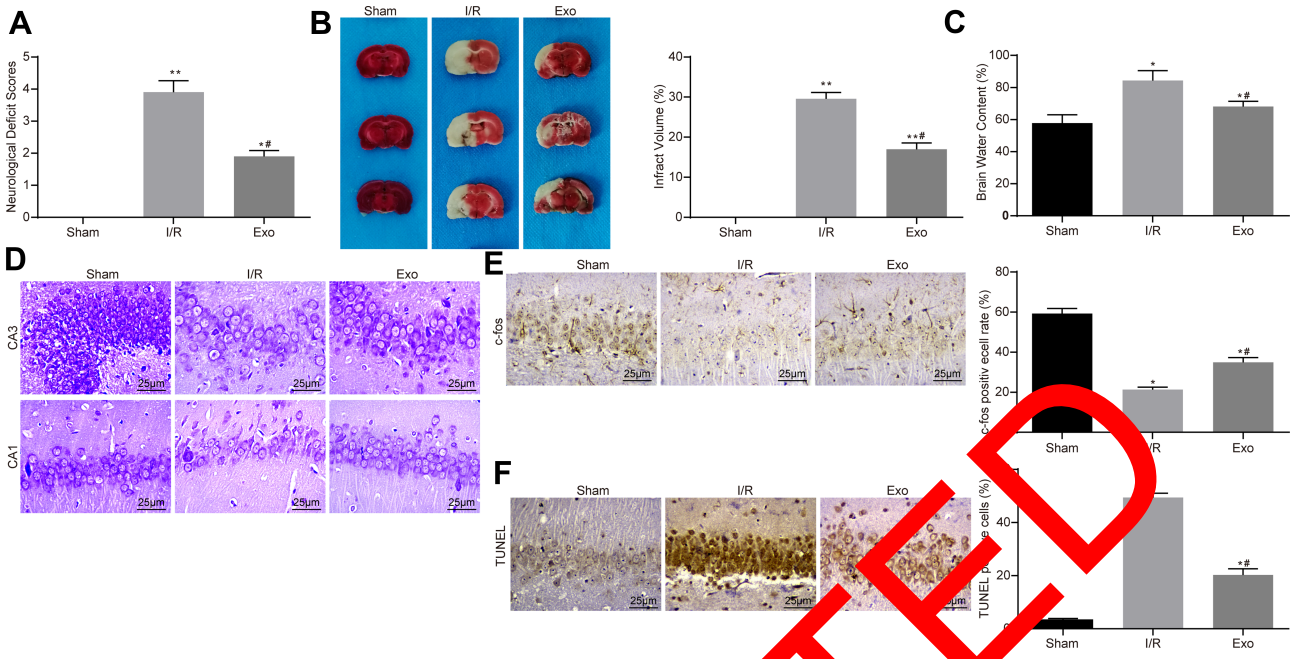

Figure 2 ATC-derived exosomes reduce I/R-induced neurological damage in rats. (**A**) After the injection of 30 μL Exo in the I/R group, the neurological deficit score was used to evaluate the effects of ATC-derived exosomes on neurocognitive function in rats. (**B**) TTC staining was used to calculate the cerebral infarct size in rats treated with exosomes. (**C**) The degree of cerebral edema was detected in rats treated with exosom (**D**) Nissl staining was used to detect the number of Nissl's body in rat brain tissue. (**E**) Detection of nerve activity in rats in each group by c-fos immunohistoche stry. (**F**) Detection of neuronal apoptosis in rats in each group by TUNEL. All experiments were performed three individual times; Data are expressed as mean ± stan rd deviation. On way ANOVA and Tukey's multiple comparison test were used to determine statistical significance. $^{*}P < 0.05$, $^{**}P < 0.01$ vs the Sham group; $^{\#}P < 0.05$ v he I/R group.
Abbreviations: ANOVA, analysis of variance; ATC, astrocyte; Exo, exosome; I/R, hemic-reperf on; TTC, 2,3,5-triphenyltetrazole chloride; TUNEL, terminal deoxynucleotidyl transferase (TdT)-mediated dUTP nick end labeling.

ATC-Derived Exosomes Pro ote Activity of OGD/R-Treate PC12 ells

The effect of simulating I/R at he ce ar level was treated by the OGD/R meth [28] The res s of MTT assay revealed that the ac ivity c cells in the OGD/R group was significant lower than at in the control group, but the ac ity of C12 cells was significantly increased following reatment wi h 30 μg/mL of ATC-derived ex s (OGD/R + Exo) (Figure 4A). The EdU st ning re lts sugg ted that exosome treatment promote the pro ion of PC12 cells (Figure 4B). Cell apopt s was detected by flow cytometry with Annexin V-FI /PI labeling. The results indicated that the addition of exosomes significantly inhibited cell apoptosis induced by OGD/R treatment (Figure 4C). Western blot analysis was performed to determine the contents of apoptosis-associated proteins Bax, Cleaved Caspase-3 and Cleaved poly-ADP-ribose polymerase (PARP) in each group, and the obtained results demonstrated that the apoptotic protein content was increased significantly following OGD/R treatment, but the contents of apoptosis-associated protein were decreased significantly following Exo treatment (Figure 4D). Furthermore, the present study performed TUNEL assay to observe the level of apoptosis and revealed that exosomal treatment decreased the amount of apoptosis in cells (Figure 4E).

ATC-Derived Exosomal *miR-361* Increases Activity of OGD/R-Treated PC12 Cell

Following treatment of PC12 cells with exosomes transfected with *miR-361* inhibitor, OGD/R treatment was performed, followed by RT-qPCR to detect the expression of *miR-361* in PC12 cells in each group, and the results revealed that the expression of *miR-361* was significantly decreased (Figure 5A). Again, the decrease in *miR-361* carried by exosomes partially reversed the protective effect of exosomes on OGD/R-treated cells. In detail, the viability of PC cells was decreased when *miR-361* was inhibited (Figure 5B), and the number of EdU-positive cells was also decreased (Figure 5C).

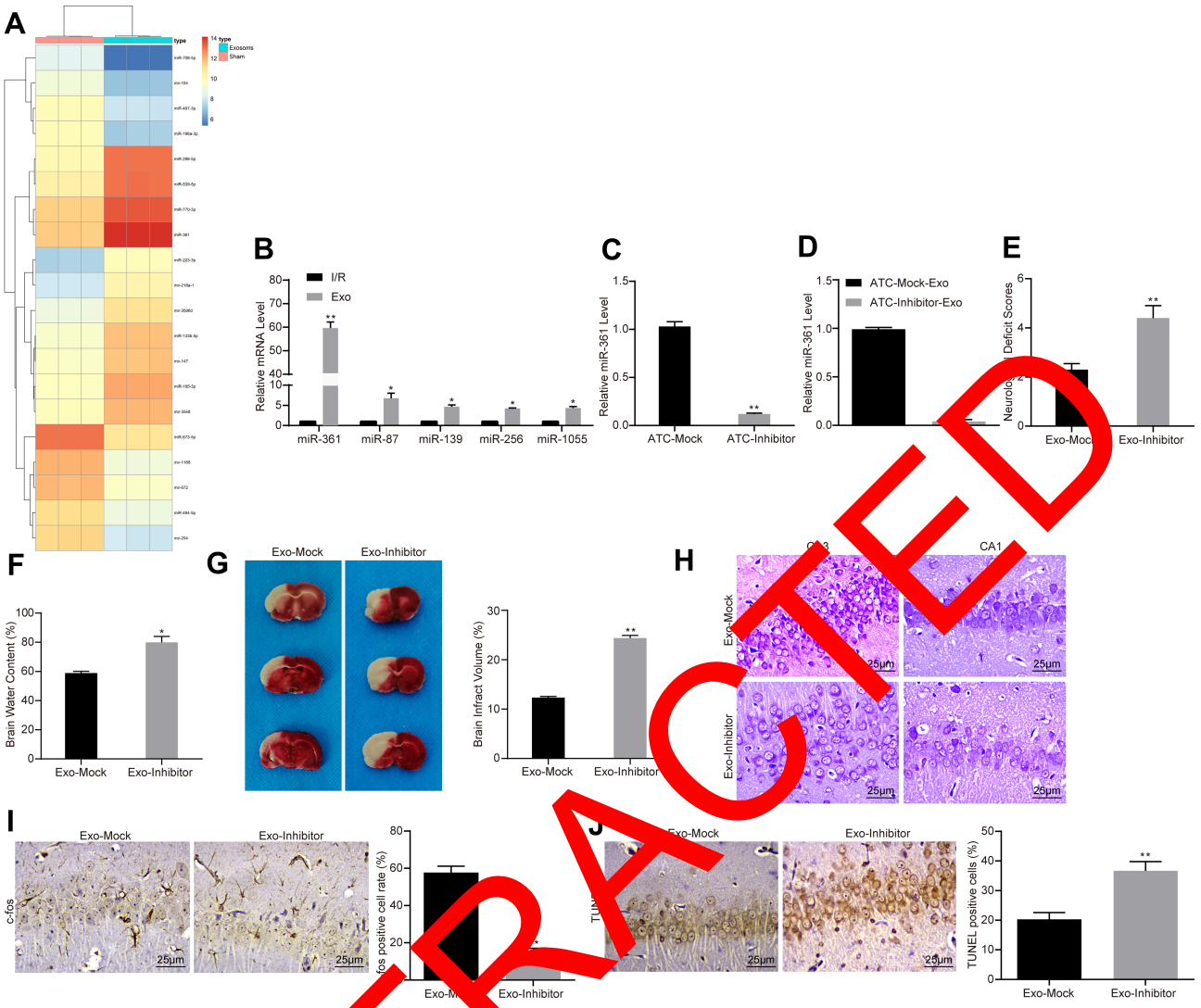

Figure 3 ATC-derived exosomal *miR-361* pr[o]tects [a]gainst injury. (**A**) We[ll] used microarray to analyze the expression of differentially expressed miRNAs in PC12 cells treated with ATC-derived exosomes. (**B**) RT-qPCR was [u]sed to detect the expression levels of *miR-361*, miR-87, miR-139, miR-256 and miR-1055 in PC12 cells to verify the accuracy of transcriptome data. (**C, D**) [E]xosomes were ex[t]racted after transfection of *miR-361* inhibitor or corresponding NC in ATCs. RT-qPCR was used to detect the expression of *miR-361* in ATCs and e[x]osomes. (**E**) I/R rats wer[e] treated with exosomes transfected with *miR-361* inhibitor or empty, at a dose of 30 μg/mL. The effect of the intervention of *miR-361* expressio[n] on the neu[r]ocognitive function of the rats was assessed by neurological deficit score. (**F, G**) The infarct size and cerebral edema degree of rats treated with *miR-361* inh[i]bitor-transf[e]cted exosomes were calculated by TTC staining. (**H**) Nissl staining used to detect the number of Nissl's body in rat brain tissue. (**I**) Detection of nerve activity in [r]ats i[n] each group [b]y c-fos immunohistochemistry. (**J**) Detection of neuronal apoptosis in rats in each group by TUNEL assay. All experiments were perfo[r]med three in[d]ividual times; [d]ata are expressed as mean ± standard deviation. One-way ANOVA and Tukey's multiple comparison test were used to determine statistical [s]ignifica[n]ce. $^{*}P < 0.$ $^{**}P <$ [0]1 vs the Exo-Mock group.

Abbreviations: [A]NOVA, an[a]lysis of varia[n]ce; ATC, astrocyte; Exo, exosome; miR, microRNA; I/R, ischemic-reperfusion; RT-qPCR, reverse transcription-quantitative polymerase cha[i]n reaction; T[T]C, 2,3,5-triphenyltetrazolium chloride; TUNEL, terminal deoxynucleotidyl transferase (TdT)-mediated dUTP nick end labeling.

Inhibition of *miR-361* in ATC-derived exosomes led to an increase in cell apoptosis according to the flow cytometry (Figure 5D). In addition, the expression levels of pro-apoptotic factors including Bax, Cleaved caspase-3 and Cleaved PARP were increased (Figure 5E). The TUNEL results also suggested an increase in the number of apoptotic cells after *miR-361* inhibition (Figure 5F)

miR-361 Plays a Neuroprotective Role by Targeting *CTSB*

To further determine the downstream mechanism of *miR-361*, the present study used TargetScan to predict the potential target gene, *CTSB* (Figure 6A). Subsequently, the present study performed a dual-luciferase reporter gene assay and the results demonstrated that *miR-361*

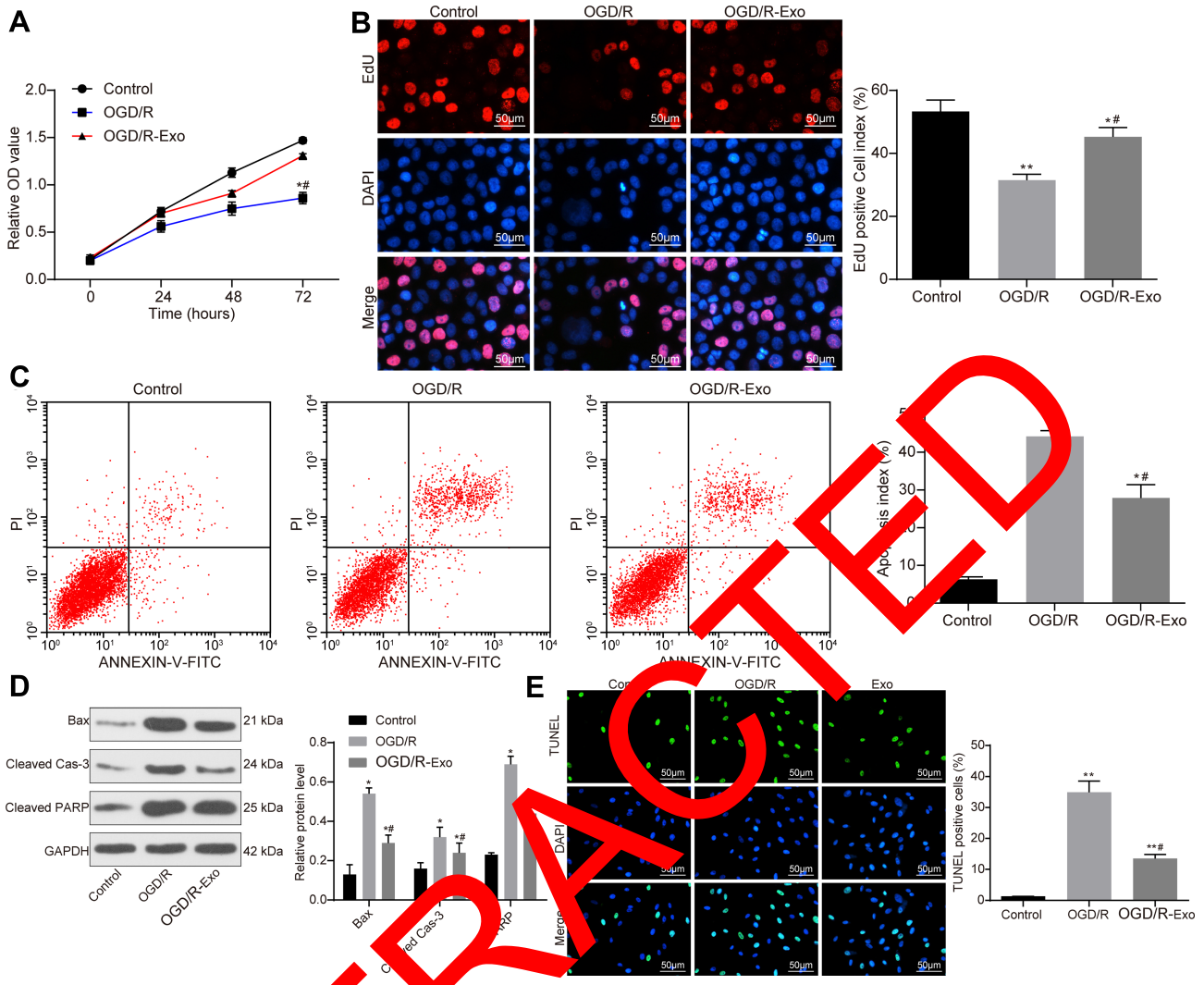

Figure 4 ATC-derived promotes OGD/R-[illegible]ed PC12 cell a[illegible]ty. (**A**) Cells were treated with OGD/R to simulated I/R at a cellular level. Measurement of cell viability using MTT assay after addition of 30 μg/[illegible] Exo[illegible] PC12 cells in th[illegible]OGD/R group. (**B**) Detection of the number of proliferating cells by EdU staining. (**C**) After PI/Annexin V FITC double-labeling, the number of apoptosis v[illegible] detected by flow cytometry. (**D**) Western blot analysis was performed to determine the contents of apoptosis-related proteins Bax, Cleaved Caspase-3[illegible]d Cleaved PARP[illegible] each group. (**E**) Apoptosis of PC12 cells in each group was detected by TUNEL assay. All experiments were performed three individual ti[illegible]. Data are expressed [illegible]ean ± standard deviation. One-way ANOVA and Tukey's multiple comparison test were used to determine statistical significance. *P < [illegible]5, **P < 0.[illegible] vs the Control group; #P < 0.05 vs the OGD/R group.

Abbreviations: ANOV[illegible]nalysis of[illegible]riance; ATC, astrocyte; Bax, Bcl-2-associated X; EdU, 5-ethynyl-2′-deoxyuridine; Exo, exosome; I/R, ischemic-reperfusion; FITC, fluorescein isothiocyanate; [illegible]PDH[illegible]glyceraldeh[illegible]e-3-phosphate dehydrogenase; MTT, 3-(4, 5-dimethylthiazol-2-yl)-2, 5-diphenyltetrazolium bromide; OGD/R, oxygen-glucose deprivatio[illegible]xygenati[illegible]PARP, poly[illegible]ADP-ribose) polymerase; PI, propidium iodide; TUNEL, terminal deoxynucleotidyl transferase (TdT)-mediated dUTP nick end labeling.

could target[illegible]he 3′-UTR sequence of *CTSB* (Figure 6B). We found that[illegible]er OGD/R treatment, the *CTSB* expression in PC12 cells was notably increased (Figure 6C). ATC-derived exosomes significantly inhibited *CTSB* expression, but this inhibition was blocked when *miR-361* was suppressed (Figure 6D). Next, in order to determine the involvement of *CTSB* in the neuroprotective events mediated by *miR-361*, the present study performed a functional rescue experiment by overexpressing *CTSB* in exosomal-treated PC12 cells. The results revealed that in OGD/R-treated PC12 cells, overexpression of *CTSB* partially offsets the protective effect of exosomes on PC cells. The viability and proliferation of PC12 cells were decreased after CTSB overexpression (Figure 6E and F), and the number of EdU-positive cells was decreased (Figure 6G). In addition, the flow cytometer results also found that the number of apoptotic cells was notably increased (Figure 6H), and the protein levels of Bax, Cleaved Caspase-3 and Cleaved PARP were increased upon *CTSB* overexpression (Figure 6I).

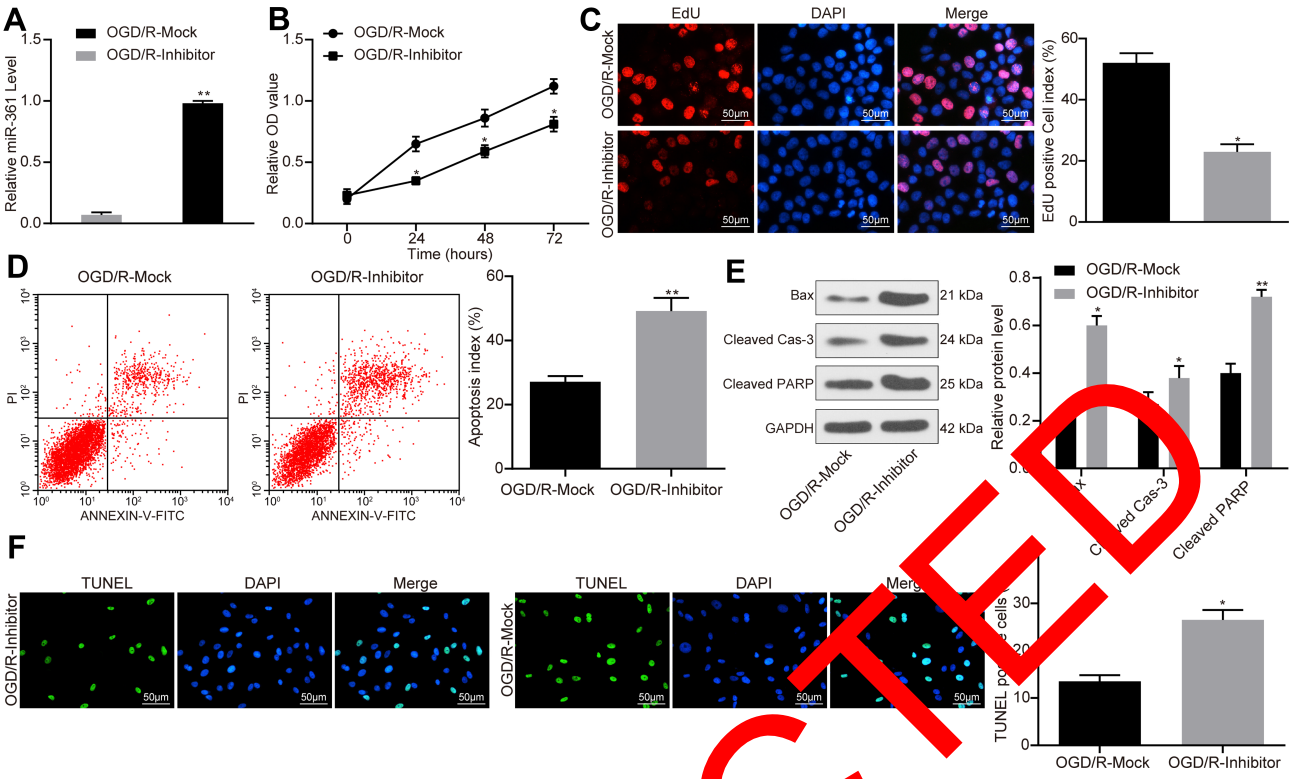

Figure 5 ATC-derived exosomal *miR-361* increases OGD/R-treated PC12 cell activity. (**A**) OGD/R-treated PC12 cells were treated with exosomes transfected with *miR-361* inhibitor or Mock at a dose of 30 μg/mL, and the expression of *miR-361* in each group was detected by RT-qPCR. (**B**) Measurement of cell viability using MTT assay. (**C**) Detection of number of proliferating cells by EdU staining. (**D**) After Annexin V-FITC/PI labeling, the number of apoptosis was detected by flow cytometry. (**E**) Western blot analysis was performed to determine the contents of apoptosis-related proteins Bax, Cleaved Caspase-3 and Cleaved PARP in each group. (**F**) Apoptosis of PC12 cells in each group was detected by TUNEL assay. All experiments were performed three individual. Data are expressed as mean ± standard deviation. One-way ANOVA and Tukey's multiple comparison test were used to determine statistical significance, while in panel B and F, two-way ANOVA was used. $^{*}P < 0.05$, $^{**}P < 0.01$ vs the OGD/R-Mock group.

Abbreviations: ANOVA, analysis of variance; ATC, astrocyte; Bcl-2-associated X; DAPI, 4′,6-diamidino-2-phenylindole; EdU, 5-ethynyl-2′-deoxyuridine; Exo, exosome; FITC, fluorescein isothiocyanate; GAPDH, glyceraldehyde-3-phosphate dehydrogenase; miR, microRNA; MTT, 3-(4, 5-dimethylthiazol-2-yl)-2, 5-diphenyltetrazolium bromide; OGD/R, oxygen-glucose deprivation/reoxygenation; PI, propidium iodide; RT-qPCR, reverse transcription-quantitative polymerase chain reaction; PARP, poly (ADP-ribose) polymerase; TUNEL, terminal deoxynucleotidyl transferase (TdT)-mediated dUTP nick end labeling.

ATC-Derived Exosomal *miR-361* Downregulates *AMPK/mTOR* Signaling Pathway by Targeting *CTSB*

The present study used RT-qPCR and Western blot analysis to detect the activation level of the *AMPK/mTOR* signaling pathway in rat brain tissues and PC12 cells. It was revealed that I/R treatment promoted the mRNA and protein levels of *AMPK/mTOR* signaling pathway cytokines in rat brain tissues. The exosome treatment reduced the activation in brain tissues, but this reduction was blocked when *miR-361* was inhibited (Figure 7A and B). Similarly, activation of *AMPK/mTOR* was observed in OGD/R-treated PC12 cells. Exosome treatment was found to suppress the mRNA and protein levels of *AMPK* and *mTOR* in cells. But these changes were reversed when upon miR-161 inhibition (Figure 7C and D).

Discussion

Various miRNAs have been demonstrated to be loaded by exosomes, which have been revealed to play roles in both inflammation and neuron injury.[29] Evidence has also revealed that exosomes secreted from ATCs exhibit protection in Huntington's disease.[30] Nevertheless, the functions of ATC-derived exosomes and the transfer of the cargo of exosomal protein and RNA have rarely been investigated in cerebral I/R injury. Based on this, the present study aimed to elucidate this issue.

The results of the present study suggested that ATC-derived exosomes decrease I/R-induced neurological damage in rats. In addition, ATC-derived exosomes promote OGD/R-treated PC12 cell activity while inhibiting its apoptosis. It is reported that exosomes are of significance in intercellular communication in the brain through the transfer of the cargo of exosomal protein and RNA

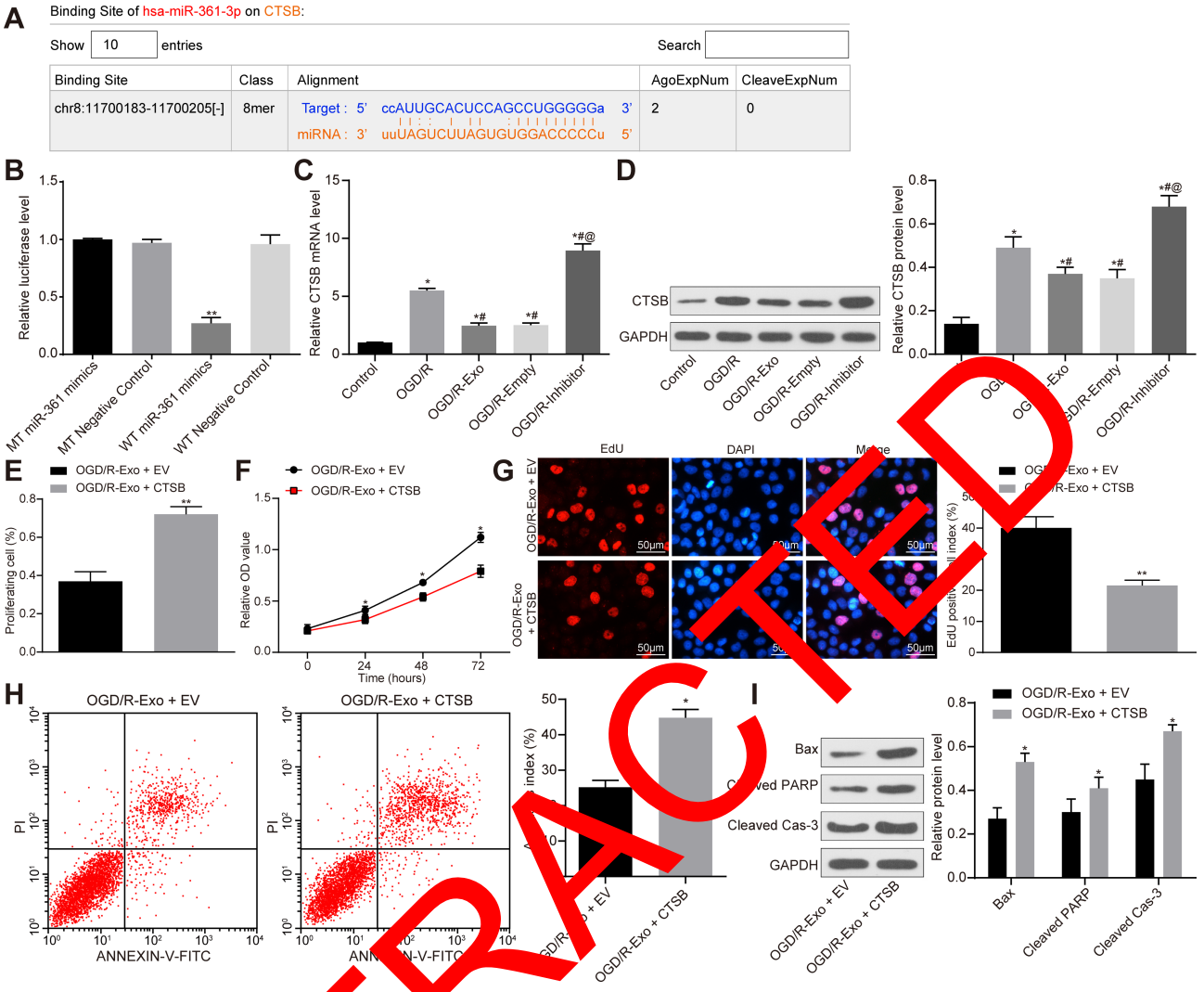

Figure 6 *miR-361* plays a neuroprotective [illegible] by targeting *CTSB*. (**A**) Starbase suggests that *miR-361* targets the 3′-UTR sequence of the *CTSB* gene. (**B**) Dual-luciferase reporter gene assay was conducted to [illegible] the target relationship between *miR-361* and *CTSB*. N = 3; * compares to WT-negative control group. (**C, D**) *CTSB* mRNA and protein levels in each group of cells. N = 3; * compares to Control group; # compares to OGD/R group; @ compares to OGD/R-Mock group. *CTSB* overexpression vector or the empty vector (EV) were transfected into exosome-treated PC12 cells, and the cells were treated with OGD/R. (**E**) measurement of cell proliferation by flow cytometry. (**F**) Measurement of cell viability using MTT assay. (**G**) Detection of the number of proliferating cells by EdU staining. (**H**) After Annexin V-FITC/PI labeling, the number of apoptosis was detected by flow cytometry. (**I**) Western blot analysis was performed to determine the contents of apoptosis-related proteins Bax, Cleaved Caspase-3 and Cleaved PARP in each group. All experiments were performed three individual times; Data are expressed as mean ± standard deviation. One-way ANOVA and Tukey's multiple comparisons test were used to determine statistical significance, while in panel D, F and I, two-way ANOVA was used. *$P < 0.05$, **$P < 0.01$ vs the OGD/R-Exo + EV group.

Abbreviations: ANOVA, analysis of variance; Bax, Bcl-2-associated X; *CTSB*, cathepsin B; EdU, 5-ethynyl-2′-deoxyuridine; EV, empty vector; FITC, fluorescein isothiocyanate; GAPDH, glyceraldehyde-3-phosphate dehydrogenase; miR, microRNA; MT, mutant type; MTT, 3-(4, 5-dimethylthiazol-2-yl)-2, 5-diphenyltetrazolium bromide; OGD/R, oxygen-glucose deprivation/reoxygenation; PI, propidium iodide; PARP, poly (ADP-ribose) polymerase; WT, wild type.

between both source and target cells.[31] The function of exosomes in cardioprotection reflects the exosomes' common function in tissue repair, and varying cell types secret exosomes, which are proprietary for the specially appointed type of cells or injuries.[32] Meanwhile, a study has indicated that exosomes have the ability to repair injured tissue, including myocardial I/R injury.[33] Given their unique properties, such as high delivery efficiency, innate stability, low immunogenicity, as well as the ability to cross the blood-brain barrier, exosomes play vital parts in treating cerebral ischemia. However, the insufficient targeting capability of exosomes restricts their clinical applications.[34] Exosomes have been demonstrated to be released from numerous types of cells, such as neurons and ATCs. It is suggested that amyloid-β abates the release of exosomes from ATCs through enhancing JNK phosphorylation.[35] As previously described, ATC-derived exosomes have a protective role in hypoxic-ischemic

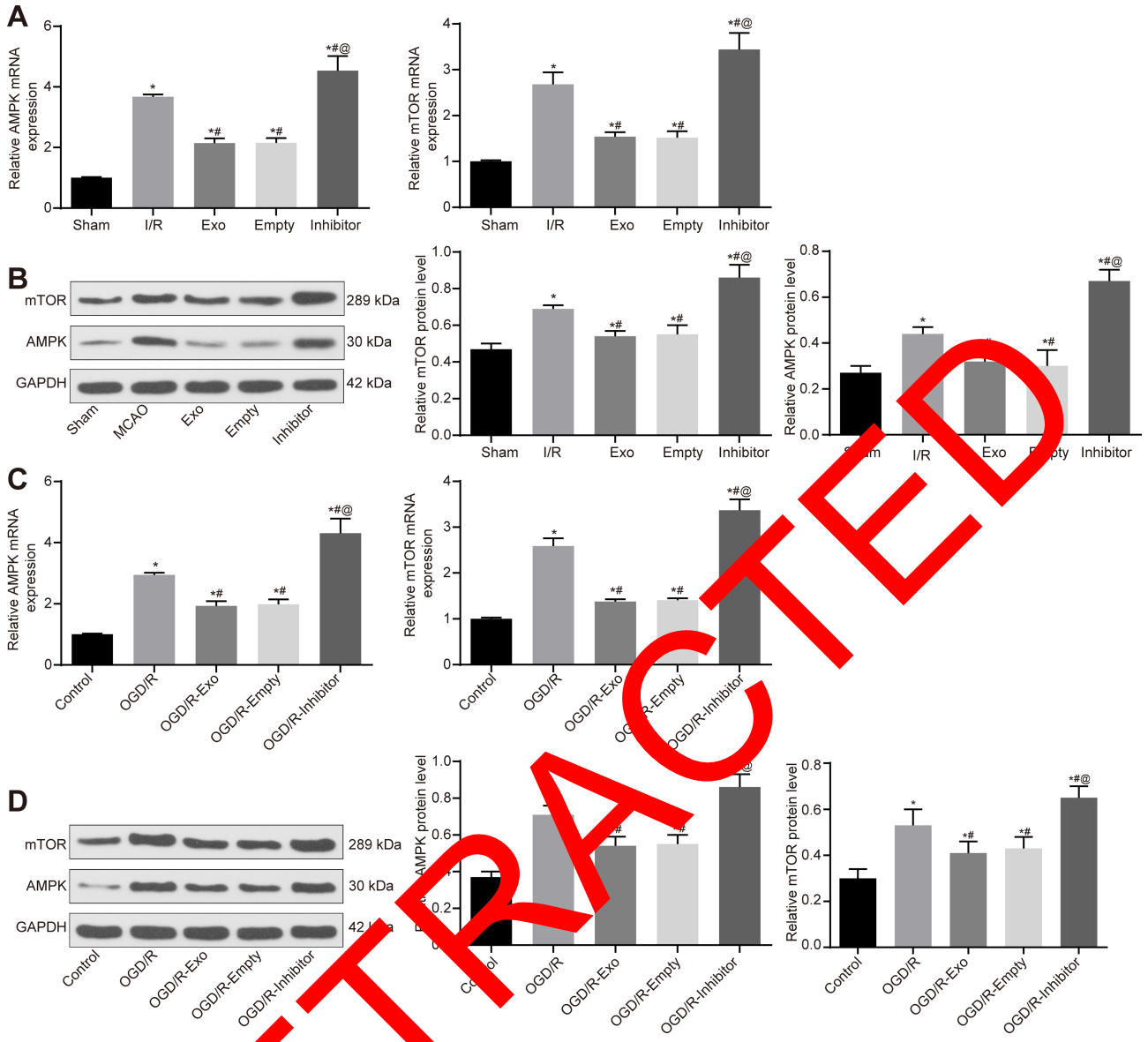

Figure 7 ATC-derived exosomal *miR-361* down-regulates *AMPK/mTOR* signaling pathway by targeting *CTSB*. (**A, B**) Detection of mRNA and protein levels of *AMPK* and *mTOR* in rat brain tissue by RT-qPCR and Western blot analysis, respectively. (**C, D**) Detection of mRNA and protein levels of *AMPK* and *mTOR* in PC12 cells by RT-qPCR and Western blot analysis, respectively. All experiments were performed three individual times; Data are expressed as mean ± standard deviation. One-way ANOVA and Tukey's multiple comparison test were used to determine statistical significance, while in panel B and D, two-way ANOVA was used. N = 3; * compares to the Sham or Control group; # compares to I/R or OGD/R group; @ compares to Empty or OGD/R-Empty group. $^{*}P < 0.05$, $^{\#}P < 0.05$, $^{@}P < 0.05$.

Abbreviations: *AMPK/mTOR*, AMP-activated protein kinase/mammalian target of rapamycin; ANOVA, analysis of variance; ATC, astrocyte; *CTSB*, cathepsin B; Exo, exosome; I/R, ischemic-reperfusion; miR, microRNA; OGD/R, oxygen-glucose deprivation/reoxygenation; RT-qPCR, reverse transcription-quantitative polymerase chain reaction.

neurons.[36] Other articles have demonstrated that ATCs with Aβ peptides treatment, or ATCs-exosomes in mice overexpressing mutant copper-zinc SOD1, are able to induce ATC apoptosis and motor neuron death, respectively.[37,38]

The present study also revealed that ATC-derived exosomal *miR-361* protects I/R injury. Exosomes secreted from various cells could stimulate neuroprotection and neurorestorative functions through regulating gene, protein and miRNA expression in their target tissues and cells.[39] It has been revealed that the modulation of *miR-361* expression also influences mitochondrial fission, apoptosis, as well as myocardial infarction.[15] *miR-361-5p*, one of the important miRNAs, has been shown to act as a tumor inhibitor in various types of tumor.[40] Zhang et al have reported that *miR-361-5p* contributes to suppressed epithelial-to-

mesenchymal transition in glioma cells via targeting Twist1.[41] Wang et al. suggested that *miR-361-5p*/vascular endothelial growth factor-dependent regulation could be new therapeutic modalities both for ischemia-associated diseases and for tumor angiogenesis.[42] In addition, *miR-361* has been identified as an apoptosis promoter regarding cancer cells in several malignancies,[43,44] though, it has been documented to decrease apoptosis of cardiomyocytes following myocardial I/R injury.[45] The present study identified a similar anti-apoptosis role of *miR-361* in neuronal apoptosis since knockdown of *miR-361* led to increased apoptosis of PC12 cells.

Furthermore, another finding was that ATC-derived exosomal *miR-361* downregulates *AMPK/mTOR* by targeting *CTSB*. *CTSB* is released from lysosomes in reperfusion-free acute focal ischemia, revealing that lysosomal destabilization could in part to lead to cerebral infarction.[46] Anagli et al. observed *CTSB* decrease and heat shock protein level decrease following cysteine protease inhibitor treatment, implying that the cysteine protease pathways are destructive at the beginning of ischemic brain injury.[47] Xing et al. also reported that the activated *CTSB* in an ischemic stroke model was markedly elevated following cortical ischemic stroke, and it may be a controller of poststroke secondary degeneration.[48] The *AMPK/mTOR* pathway is significant in autophagy modulation in response to both stres[illegible]lucose starvation. Augmenter of liver regenerati[illegible] regulates [illegible]tophagy level through the *AMPK/mTOR* pa[illegible]way in re[illegible]l I/R injury, which could functi[illegible] as an [illegible]ntioxi[illegible]ant protein.[49] However, these re[illegible]lts requi[illegible]e furth[illegible]erification due to the lack of rela[illegible]ve [illegible]cu[illegible]ents.

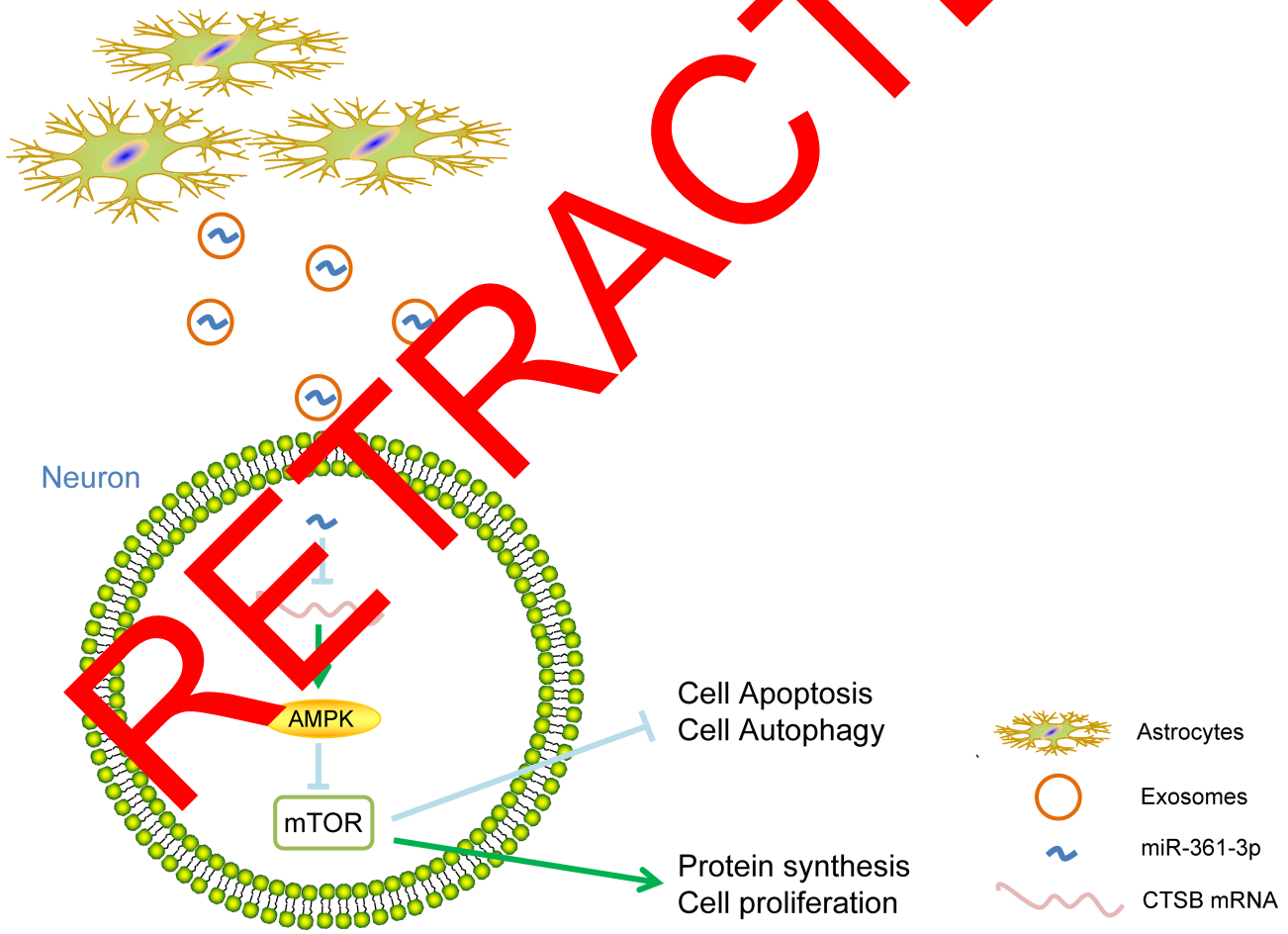

Figure 8 The mechanistic diagram highlights that ATCs-derived exosomal *miR-361* downregulates *AMPK/mTOR* signaling pathway by binding to *CTSB* to reduce nerve damage caused by I/R.

Abbreviations: ATC, astrocyte; miR, microRNA; *AMPK/mTOR*, AMP-activated protein kinase/mammalian target of rapamycin; *CTSB*, cathepsin B; I/R, ischemic-reperfusion.

Conclusion

Overall, the present study highlights that ATCs-derived exosomal *miR-361* downregulates the *AMPK/mTOR* signaling pathway by binding to *CTSB* to decrease nerve damage caused by I/R (Figure 8). Therefore, exosomes may be utilized as a special targeted drug delivery vehicle. Furthermore, the present study could shed new light on the miRNA-based therapy for cerebral I/R injury.

Disclosure

The authors declare no potential conflicts of interest.

References

1. Liu Y, Ma Y, Zhang B, Wang SX, Wang XM, Yu JM. Genetic polymorphisms in pre-microRNAs and risk of ischemic stroke in a Chinese population. *J Mol Neurosci*. 2014;52(4):473–480.
2. Maddahi A, Kruse LS, Chen QW, Edvinsson L. The role of tumor necrosis factor-alpha and TNF-alpha receptors in cerebral arteries following cerebral ischemia in rat. *J Neuroinflammation*. 2011;8(1):107. doi:10.1186/1742-2094-8-107
3. Yan RY, Wang SJ, Yao GT, Liu ZG, Xiao N. The protective effect and its mechanism of 3-n-butylphthalide pretreatment on cerebral ischemia reperfusion injury in rats. *Eur Rev Med Pharmacol Sci*. 2017;21(22):5275–5282. doi:10.26355/eurrev_201711_13852
4. Xu F, Ma R, Zhang G, et al. Estrogen and propofol combination therapy inhibits endoplasmic reticulum stress and remarkably attenuates cerebral ischemia-reperfusion injury and OGD injury hippocampus. *Biomed Pharmacother*. 2018;108:1596–1606. doi:10.1016/j.biopha.2018.09.167
5. Al-Mufti F, Amuluru K, Roth W, Nuoman R, [illegible] M, Meyers PM. Cerebral ischemic reperfusion injury following recanalization of large vessel occlusions. *Neurosurgery*. [illegible] (6):781–789. doi:10.1093/neuros/nyx341
6. Wu PF, Zhang Z, Wang F, Chen JG. Natural compounds from traditional medicinal herbs in the treatment of cerebral ischemia/reperfusion injury. *Acta Pharmacol Sin*. 2010;31(12):[illegible] doi:10.1038/aps.2010.186
7. Cetin C, Erdogan AM, Dincel GC, Bakar E, Kisa U. Effects of sulphasalazine in cerebral ischemia reperfusion injury in rat. *Arch Med Res*. 2017;48(3):247–256. doi:10.1016/j.arcmed.2017.06.004
8. Gyorgy B, Hung ME, Breakefield XO, Leonard JN. Therapeutic applications of extracellular vesicles: clinical promise and open questions. *Annu Rev Pharmacol Toxicol*. 2015;55(1):439–464. doi:10.1146/annurev-pharmtox-010814-124630
9. Lai CP, Breakefield XO. Role of exosomes/microvesicles in the nervous system and emerging therapies. *Front Physiol*. 2012;3:228. doi:10.3389/fphys.2012.00228
10. Deng M, Xiao H, Zeng H, et al. Preservation of neuronal functions by exosomes derived from different human neural cell types under ischemic conditions. *Eur J Neurosci*. 2018;47(2):150–157. doi:10.1111/ejn.13784
11. Xian P, Hei Y, Wang R, et al. Mesenchymal stem cell-derived exosomes as a nanotherapeutic agent for amelioration of inflammation-induced astrocyte alterations in mice. *Theranostics*. 2019;9(20):5956–5975. doi:10.7150/thno.33872
12. Nafar F, Williams JB, Mearow KM. Astrocytes release HspB1 in response to amyloid-beta exposure in vitro. *J Alzheimers Dis*. 2016;49(1):251–263. doi:10.3233/JAD-150317
13. Taylor AR, Robinson MB, Gifondorwa DJ, Tytell M, Milligan CE. Regulation of heat shock protein 70 release in astrocytes: role of signaling kinases. *Dev Neurobiol*. 2007;67(13):1815–1829. doi:10.1002/dneu.20559
14. Yu H, Wu M, Zhao P, Huang Y, Wang W, Yin W. Neuroprotective effects of viral overexpression of microRNA-22 in rat and cell models of cerebral ischemia-reperfusion injury. *J Cell Biochem*. 2015;116(2):233–241. doi:10.1002/jcb.24960
15. Wang K, Liu CY, Zhang XJ, et al. miR-361-regulated prohibitin inhibits mitochondrial fission and apoptosis and protects heart from ischemia injury. *Cell Death Differ*. 2015;22(6):1058–1068. doi:10.1038/cdd.2014.200
16. Kar S, Bali KK, Baisantry A, Geffers R, Samii A, Bertalanffy H. Genome-wide sequencing reveals MicroRNAs downregulated in cerebral cavernous malformations. *J Mol Neurosci*. 2017;61(2):178–188. doi:10.1007/s12031-017-0880-6
17. Iwakawa HO, Tomari Y. The Functions of MicroRNAs: mRNA Decay and Translational Repression. *Trends Cell Biol*. 2015;25(11):651–665. doi:10.1016/j.tcb.2015.07.011
18. Ozden H, Durmaz R, Kanbak G, et al. Erythropoietin prevents nitric oxide and cathepsin-mediated neuronal death in focal brain ischemia. *Brain Res*. 2011;1370:185–193. doi:10.1016/j.brainres.2010.11.045
19. Zuo X, Hou Q, Jin J, et al. Inhibition of cathepsin B alleviates secondary degeneration in ipsilateral thalamus after focal cerebral infarction in adult rat. *J Neuropathol Exp Neurol*. 2016;75(9):816–826. doi:10.1093/jnen/nlw054
20. Thompson CA, Purushothaman A, Ramani VC, Vlodavsky I, Sanderson RD. Heparanase regulates secretion, composition, and function of tumor cell-derived exosomes. *J Biol Chem*. 2013;288(14):10093–10099. doi:10.1074/jbc.C112.444562
21. Longa EZ, Weinstein PR, Carlson S, Cummins R. Reversible middle cerebral artery occlusion without craniectomy in rats. *Stroke*. 1989;20(1):84–91. doi:10.1161/01.STR.20.1.84
22. Yan Z, Lin Y, Jing J, Qiu Y, Ren L. Expression and functions of glutamate and gamma-aminobutyric acid transporters in ischemic mod[illegible] *Mol Med Rep*. 2018;17(6):8196–8202. doi:10.3892/mmr.2018.[illegible]
23. [illegible] Z, Weian C, Susu H, Hanmin W. Protective effects of mangiferin on cerebral ischemia-reperfusion injury and its mechanisms. *Eur J Pharmacol*. 2016;771:145–151. doi:10.1016/j.ejphar.2015.12.003
24. Gutierrez IL, Gonzalez-Prieto M, Garcia-Bueno B, Caso JR, Leza JC, Madrigal JLM. Alternative method to detect neuronal degeneration and amyloid beta accumulation in free-floating brain sections with fluoro-jade. *ASN Neuro*. 2018;10:1759091418784357. doi:10.1177/1759091418784357
25. Tian SF, Yang HH, Xiao DP, et al. Mechanisms of neuroprotection from hypoxia-ischemia (HI) brain injury by up-regulation of cytoglobin (CYGB) in a neonatal rat model. *J Biol Chem*. 2013;288(22):15988–16003. doi:10.1074/jbc.M112.428789
26. Chinenov Y, Kerppola TK. Close encounters of many kinds: fos-Jun interactions that mediate transcription regulatory specificity. *Oncogene*. 2001;20(19):2438–2452. doi:10.1038/sj.onc.1204385
27. Rawat V, Goux W, Piechaczyk M, Dm SR. c-Fos protects neurons through a noncanonical mechanism involving HDAC3 interaction: identification of a 21-Amino acid fragment with neuroprotective activity. *Mol Neurobiol*. 2016;53(2):1165–1180. doi:10.1007/s12035-014-9058-1
28. Tao T, Feng JZ, Xu GH, Fu J, Li XG, Qin XY. Minocycline promotes neurite outgrowth of PC12 cells exposed to oxygen-glucose deprivation and reoxygenation through regulation of MLCP/MLC Signaling pathways. *Cell Mol Neurobiol*. 2017;37(3):417–426. doi:10.1007/s10571-016-0374-z
29. Deng Y, Chen D, Gao F, et al. Exosomes derived from microRNA-138-5p-overexpressing bone marrow-derived mesenchymal stem cells confer neuroprotection to astrocytes following ischemic stroke via inhibition of LCN2. *J Biol Eng*. 2019;13(1):71. doi:10.1186/s13036-019-0193-0
30. Hong Y, Zhao T, Li XJ, Li S. Mutant Huntingtin Inhibits alphaB-Crystallin Expression and Impairs Exosome Secretion from Astrocytes. *J Neurosci*. 2017;37(39):9550–9563. doi:10.1523/JNEUROSCI.1418-17.2017

31. Zhang ZG, Chopp M. Exosomes in stroke pathogenesis and therapy. *J Clin Invest*. 2016;126(4):1190–1197. doi:10.1172/JCI81133
32. Lai RC, Arslan F, Lee MM, et al. Exosome secreted by MSC reduces myocardial ischemia/reperfusion injury. *Stem Cell Res*. 2010;4(3):214–222. doi:10.1016/j.scr.2009.12.003
33. Sze SK, de Kleijn DP, Lai RC, et al. Elucidating the secretion proteome of human embryonic stem cell-derived mesenchymal stem cells. *Mol Cell Proteomics*. 2007;6(10):1680–1689. doi:10.1074/mcp.M600393-MCP200
34. Tian T, Zhang HX, He CP, et al. Surface functionalized exosomes as targeted drug delivery vehicles for cerebral ischemia therapy. *Biomaterials*. 2018;150:137–149. doi:10.1016/j.biomaterials.2017.10.012
35. Abdullah M, Takase H, Nunome M, et al. Amyloid-beta reduces exosome release from astrocytes by enhancing JNK phosphorylation. *J Alzheimers Dis*. 2016;53(4):1433–1441. doi:10.3233/JAD-160292
36. Huang JL, Qu Y, Tang J, et al. [Protective effect of astrocyte exosomes on hypoxic-ischemic neurons]. *Zhongguo Dang Dai Er Ke Za Zhi*. 2018;20(5):397–402. Chinese.
37. Basso M, Pozzi S, Tortarolo M, et al. Mutant copper-zinc superoxide dismutase (SOD1) induces protein secretion pathway alterations and exosome release in astrocytes: implications for disease spreading and motor neuron pathology in amyotrophic lateral sclerosis. *J Biol Chem*. 2013;288(22):15699–15711. doi:10.1074/jbc.M112.425066
38. Wang G, Dinkins M, He Q, et al. Astrocytes secrete exosomes enriched with proapoptotic ceramide and prostate apoptosis response 4 (PAR-4): potential mechanism of apoptosis induction in Alzheimer disease (AD). *J Biol Chem*. 2012;287(25):21384–21395. doi:10.1074/jbc.M112.340513
39. Chen J, Chopp M. Exosome Therapy for Stroke. *Stroke*. 2018;49(5):1083–1090. doi:10.1161/STROKEAHA.117.018292
40. Tian L, Zhao Z, Xie L, Zhu J. MiR-361-5p suppresses chemoresistance of gastric cancer cells by targeting FOXM1 via the PI3K/Akt/mTOR pathway. *Oncotarget*. 2018;9(4):4886–4896. doi:10.18632/oncotarget.23513
41. Zhang X, Wei C, Li J, Liu J, Qu J. MicroRNA-361-5p [illegible] its epithelial-to-mesenchymal transition of glioma cells through [illegible]rgeting Twist1. *Oncol Rep*. 2017;37(3):1849–1856. doi:10.[illegible]892/or.2017.5406
42. Wang HW, Lo HH, Chiu YL, et al. Dysregulated miR-361-5p/VEGF axis in the plasma and endothelial progenitor cells of patients with coronary artery disease. *PLoS One*. 2014;9(5):e98070. doi:10.1371/journal.pone.0098070
43. Liu B, Lu B, Wang X, Jiang H, Kuang W. MiR-361-5p inhibits cell proliferation and induces cell apoptosis in retinoblastoma by negatively regulating CLDN8. *Childs Nerv Syst*. 2019;35(8):1303–1311. doi:10.1007/s00381-019-04199-9
44. Radunz S, Wedepohl S, Rohr M, Calderon M, Tschiche HR, Resch-Genger U. pH-Activatable Singlet Oxygen-Generating Boron-dipyrromethenes (BODIPYs) for Photodynamic Therapy and Bioimaging. *J Med Chem*. 2020;63(4):1699–1708. doi:10.1021/acs.jmedchem.9b01873
45. Xie Y, Yao FL, Li X. MicroRNA-361 regulates apoptosis of cardiomyocytes after ischemic-reperfusion injury. *Eur Rev Med Pharmacol Sci*. 2019;23(12):5413–5421. doi:10.2[illegible]rev_201906_18210
46. Benchoua A, Braudeau J, Reis[illegible], Couriat[illegible]C, Onteniente B. Activation of proinflammatory [illegible]aspases by ca[illegible]psin B in focal cerebral ischemia. *J Cereb [illegible]lood Flow [illegible]etab*. 2004;24(11):1272–1279. doi:10.1[illegible]7//01.WC[illegible]00014027[illegible]54583.FB
47. Anagli J, Abounit K, Ste[illegible]ner P, et al. Effects [illegible]ath[illegible]sins B and L inhibition on postischemic pr[illegible]n alterati[illegible] in the br[illegible]. *Biochem Biophys Res Commun*. 2008;3[illegible]6(1)[illegible]91[illegible].10.1016/j.bbrc.2007.11.104
48. Xing S, Zha[illegible] J, Dang[illegible]et al. Ce[illegible]rolysin reduces amyloid-beta deposits, [illegible]optosis and a[illegible]phag[illegible] in the thalamus and improves functi[illegible]al rec[illegible]ery after cort[illegible] infarction. *J Neurol Sci*. 2014;337(1–2):104–111. d[illegible]10.1016/j.jns.2013.11.028
49. [illegible]Liao XH, S[illegible]H, et al. Augmenter of liver regeneration regulates autophagy [illegible] renal ischemia-reperfusion injury via the AMPK/mTOR pathway. *Apoptosis*. 2017;22(7):955–969. doi:10.1007/[illegible]0495-017-1370-6